journal

J. Am. Ceram. Soc., **96** [7] 2132–2140 (2013)
DOI: 10.1111/jace.12402

A Nondestructive Methodology for the Study of Colored Enamels: Insights into Manufacturing and Weathering Processes

Julia Romero-Pastor,[‡,†] José Vicente Navarro,[§] Marian del Egido,[§] and Miguel Ortega-Huertas[‡]

[‡]Dept. of Mineralogy and Petrology, University of Granada, Granada 18002, Spain

[§]Instituto del Patrimonio Cultural de España, Madrid 28040, Spain

We studied ancient enamels on gilded copper from a collection of archeological horse harness pendants of the *Museo Instituto Valencia de Don Juan* (Madrid, Spain) to test the benefits of a new, nondestructive analytical methodology based on chemometric analysis (i.e., Principal Component Analysis, PCA) on micro-ATR-FTIR spectral data and chemical quantification using SEM-EDS. The novelty of this approach was threefold: (i) PCA allowed the discrimination of the different harness pendants of known origin and attributed to the 14th and 15th centuries according to the chemical complex composition, nanostructure, glass weathering, and/or coloring mechanisms of each colored enamel, separately (i.e., red, purple, blue, and white), (ii) it is a cheap, easily available and nondestructive methodology that enables us to (iii) draw archeological conclusions about the quality of the manufacturing process, reassess the chronology of these objects and attempt to attribute them to different workshops according to the different traditional recipes identified. In particular, the enamels were made of alkali and/or alkaline earth lead-glass with a wide range of chemical compounds in the form of pigments or opacifiers. Two types of coloring mechanisms were identified, colloidal particles such as copper-ruby for red enamels, and ionic mechanisms such as Fe(II) and Co(II) to achieve a blue pigments; Mn(III) in the purple pigment; and two kind of white enamels were identified, i.e., tin oxide as an opacifier and uranium oxide. In addition, we established the reason for the poor state of conservation of some of the enamels by means of the identification of depolymerization and ion exchanges, well-known harmful effects of glass weathering, and finally a chronology was assigned for some of these pieces according to the enamel composition.

I. Introduction

Studies of the structure and of the weathering of glass or enamels (i.e., champlevé) normally require the use of a wide range of advanced analytical techniques that enable us to explore their chemical composition and alteration mechanisms. However, these techniques are often expensive or not easily available, e.g., Particle Induced X-Ray (PIXE), Gamma Ray Emission (PIGE), portable X-Ray Fluorescence (p-XRF), or analytical techniques based on synchrotron radiation.[1–4] There are other techniques which are quite unsuitable for the study of whole archeological objects because they require samples to be taken from the object and prepared for analysis (often involving grinding), so damaging or destroying the object (e.g., Transmission Electron Microscopy, TEM; X-Ray Diffraction, XRD; Nuclear Magnetic Resonance Spectroscopy, NMRS; Differential Thermal Analysis (DTA).[5–9] Moreover, the complex composition and nanostructure of ancient glass pieces, their unstable thermodynamical properties and the fact that they have no crystallographic restrictions or stoichiometric ratios mean that a detailed knowledge of properties such as color and durability can only be acquired with advanced techniques.[10]

As regards colorimetric studies of glass, invasive techniques such as TEM, XRD, or FTIR revealed that different colors were obtained using different coloring methods, i.e., by transition-metal ions (e.g., Fe, Co, Ni, Cr, Mn) or by colloidal particles or microcrystals. The metal ions produce different colors depending on their oxidation state,[11–14] while the colloidal particles or microcrystals require a heat-treatment process in reduced conditions to obtain a specific color. For the first method mentioned, the Ligand Field Theory (LFT) predicts the electronic transitions for every metal ion in octahedral or tetrahedral symmetry coloring glass using an ionic coloration mechanism.[11,12] In addition, TEM and XRD were used to identify dispersed crystals of metallic copper, characteristic of a traditional red glass called copper-ruby manufactured since Ancient Egyptian times (1500 B.C.).[5–11] However, invasive, destructive techniques similar to these clearly cannot be used on ancient objects from our archeological and historical heritage that we are seeking to preserve for posterity. These pieces which are often of great artistic value can therefore only be analyzed using nondestructive analytical methodologies.

Fortunately, there are a number of nondestructive analytical techniques (i.e., Micro-Attenuated Total Reflectance Fourier Transform Infrared Spectroscopy, micro-ATR-FTIR; Raman Microscopy, RM; Scanning Electron Microscopy Energy dispersive X-ray Spectroscopy, SEM-EDS; etc.), which can provide detailed information about corrosion processes for example, or can shed light on the different methods used in the manufacture of ancient glass.[9,15,17–22] In particular, the degree of polymerization of the glass network and as a result its structural stability were assessed using an IR/Raman profile between 1050 and 850 cm^{-1} and were found to vary depending on the content of Pb–O or the melting temperature.[15,23,24] These techniques (i.e., FTIR/RM) are complementary, and only a slight shift of the position of the vibrational bands of the silicate network is observed. This must be taken into consideration when arranging the band assignment.[24] Furthermore, the successful combination of spectroscopic techniques with chemometric evaluation has created an original way of investigating various aspects of these materials such as their characterization and the weathering processes that affect them.[25–28]

In this sense, previous research has demonstrated the benefit of applying spectral data coupled with a multivariant analysis (e.g., Principal Component Analysis, PCA) to detect structural interactions and alteration processes in painting materials.[29–31] However, very little research has been done on the combined

I. Lloyd—contributing editor

Manuscript No. 32490. Received December 17, 2012; approved April 25, 2013.
[†]Author to whom correspondence should be addressed. e-mail: juliaromero@ugr.es

use of these techniques in ancient glass and enamels. In particular, PCA was used for the discrimination of alteration processes and the division of glass pieces into groups based on different historical eras or low amounts of chromophores.[4,8,22] Previous research has shown the relation between the visual aspect of the decay suffered by an ancient glass object and its chemical composition, the range of temperatures at which the craftsmen worked, depolymerization and/or ionic exchange/depletion.[9,32–35] Indeed, the diverse oxides identified in the silicate glass from the objects provide diverse beneficial properties as network modifiers in the elaboration of high-quality glass, i.e., by increasing the mechanical and chemical resistance of the glass (e.g., calcium oxide), decreasing the fusion temperature (e.g., sodium oxide), increasing the brightness (e.g., uranium oxide), improving the development of color and also avoiding the devitrification (e.g., lead oxide).[11] However, the durability of glass when exposed to a variety of unknown environmental conditions has never been studied using chemometric approaches.

Thus, this article proposes a new nondestructive approach for studying colored enamels from ancient works of art (in this case horse harness pendants) based on the chemometric analysis of micro-ATR-FTIR spectral data and chemical quantification using SEM-EDS. The goal is to discriminate the role of diverse chemical species in the structure of the glass network, to analyze the relationship between the composition and the degree of decay and consequently, to propose a theory about the state of conservation of these objects on the basis of the state of their enamel. Our ultimate goal is to draw archeological conclusions to help clarify the origin of these works of art and attribute them to a particular historical period or even a particular enameling technique, according to the chemical composition and/or the manufacturing quality of the glass.

II. Experimental Procedure

(1) Samples

We analyzed seven horse harness pendants decorated with gilded copper. The front faces were decorated with rich-colored enamels (i.e., glass on metal) depicting coats of arms, human figures, animals, and symbols (Fig. 1). The pieces come from the archeological jewelry collection (ref. 30572) of the *Museo Instituto Valencia de Don Juan* (Madrid, Spain) and they were studied by experts from the *Instituto de Patrimonio Cultural de España* (IPCE, Spanish Cultural Heritage Institute) in Madrid, Spain. These pieces are of unknown origin and are believed to be from the 14th or 15th century. They are numbered 1 (5376), 4 (5414), 6 (5308), 7 (5601), 10 (5470), 11 (5300), and 13 (1163) according to the IPCE and museum reference systems, respectively, and contain a number of different colored enamels (red, purple, blue, and white).[37] Red enamels were used to decorate a large surface area of pendants 1, 4, 6, 7, and 11; purple enamels were used in less important surface areas in pendants no. 1, 10, and 11 and white enamels were also identified in pendants 4, 7, and 11. In addition, red, purple, and white were used as the background colors, whereas the blue enamels were reserved for decorating the more important details, i.e., clothing or coats of arms, in pendants 4, 6, 7, 11, and 13 (Fig. 1). Conservation problems typically manifest themselves in the form of cracks or chips and there are also single enamels that have both opaque and transparent glass.

(2) Analytical Techniques

We began with an overview of the enamels. We examined their morphology and color using a polarized light microscope in reflected light (Olympus SZX16). The system was equipped with a digital camera for microphotography (Olympus DP21). We then performed a detailed chemical and morphological analysis using an FTIR microspectroscopy system, an Attenuated Total Reflectance (ATR) FTIR spectrometer Bruker (Madrid, Spain) Tensor EQUINOX in conjunction with a FTIR Bruker Hyperion-2000 microscopy attachment equipped with a 20x viewing objective with a pixel resolution of 2.7 μm, equipped with CCD-camera and germanium crystal. IR spectra and optical microscope (OM) images were also registered. The spectra were measured with 4 cm^{-1} resolution and 32 scans coaddition. The spectrometer was linked to a PC equipped with Bruker OPUS 5.5 software, which collected the IR spectra. The measurements were conducted in ATR mode. Spectra were collected within the wavenumber range of 4000–600 cm^{-1} of the mid-IR region. The pendants were mounted in the sample holder and no additional sample preparation was done. We performed between 3 and 7 spectra on each colored enamel depending on the degree of alteration on the surface. We also carried out an in-depth chemical and morphological analysis using a Scanning Electron Microscope (SEM) Hitachi (Krefeld, Germany) VP-SEM S-3400N coupled with an Energy-Dispersive X-Ray Spectroscopy (EDS) microanalysis Bruker Quantax X-Flash SDD. The operating SEM-EDS conditions were from 60 to 70 pA filament current and 125 eV/ch resolution for single analyses. The beam energy used was 125 keV. Single-point elemental analyses were registered in every glass color and the same areas analyzed using Micro-ATR-FTIR; the average for the chemical quantification is shown in Table I. To identify/visualize the composition in the enamel, we then compiled ternary phase diagrams for elemental chemical quantification using the Tridraw 4.5a (Jose I. Hualde, 1996-2005) free software. We could not interpret the copper content since its origin was uncertain as the metal base of the pendants also contained copper.

Fig. 1. Images of the seven horse harness pendants we studied.

(3) Chemometric Analysis

Principal Component Analysis was performed separately on ATR-FTIR spectral data on the basis of the color of the enamels, i.e., red, purple, white, and blue to reduce its multidimensional space to extract information. In this way we built four data matrices, one for each color, which initially included the spectra of every pendant decorated with this

Table I. SEM-EDS Results of Enamels

Pendants		% Composition																
No. Ref.	Color	SiO_2	Al_2O_3	Na_2O	K_2O	MgO	CaO	P_2O_5	SO_3	Cl	Cr_2O_3	MnO	Fe_2O_3	CoO	CuO	As_2O_3	SnO_2	PbO	U
1	Red	52.9	1.2	5.9	7.0	–	2.6	0.3	–	0.2	–	1.5	2.3	–	6.1	2.3	–	20.6	–
	Purple	55.7	1.6	9.3	7.4	0.2	3.9	–	–	0.1	–	4.1	1.8	1.3	3.2	1.7	–	12.3	–
4	Red	51.0	2.2	12.2	7.0	0.1	4.6	0.2	–	0.2	–	2.4	–	5.6	2.6	–	–	11.2	
	Blue	47.5	1.0	6.4	6.6	0.1	2.3	0.5	–	0.5	–	0.5	0.5	0.3	4.3	1.5	2.2	26.5	–
	White	43.5	0.9	6.5	4.9	1.0	4.7	0.9	–	0.4	–	0.5	0.7	–	3.1	3.5	2.7	28.5	6.5
6	Red	49.2	1.4	4.9	5.6	0.3	2.5	–	–	0.3	–	0.2	4.4	–	6.0	2.2	–	24.4	
	Blue	54.8	0.8	6.2	9.7	0.5	2.1	–	–	0.3	0.4	1.2	0.9	–	3.8	1.9	–	19.2	–
7	Red	49.7	4.3	13.1	6.3	2.8	7.5	1.4	9.0	0.5	1.1	2.0	9.0	1.6	0.9	5.2	9.0	3.4	–
	Blue	51.0	2.1	13.6	3.1	1.7	4.8	0.8	–	0.6	–	0.5	2.3	0.3	1.9	0.7	8.5	8.1	–
	White	49.1	1.9	10.9	2.6	1.0	4.0	0.2	–	0.3	–	1.1	1.2	–	1.1	0.6	14.1	12.0	–
10	Purple	48.1	1.3	5.1	9.0	–	1.2	–	–	1.1	–	3.1	2.1	–	7.0	2.5	–	17.1	–
11	Red	46.2	1.1	8.0	6.7	0.2	3.2	–	–	–	0.4	0.6	2.7	Tr	11.9	1.4	–	17.7	–
	Purple	43.5	1.4	7.0	6.6	0.2	3.7	–	–	0.5	–	4.4	2.5	0.5	12.7	0.9	–	15.9	–
	Blue	46.6	0.6	4.0	9.9	0.2	3.1	0.7	–	0.3	–	2.3	1.9	1.2	4.7	1.6	–	24.5	–
	White	43.1	1.0	6.8	4.3	0.7	3.9	1.0	–	0.3	–	0.5	0.5	–	3.2	4.8	6.9	28.4	7.2
13	Blue	64.8	1.5	13.2	2.2	0.4	7.1	0.1	0.8	0.4	–	0.2	0.4	0.6	6.4	0.9	1.2	1.3	–
	White	54.0	1.7	11.7	1.4	1.5	7.0	0.2	2.9	1.4	–	–	0.5	–	11.2	1.5	2.8	2.2	–

color. The red, purple, white, and blue matrices were formed by 100, 65, 85, and 135 spectra, respectively. Enamel from 3 to 7 surface areas (identified by letters from the Latin alphabet) was analyzed depending on the visual decay, and each area was characterized by the registration of five ATR-FTIR spectra recorded under the same experimental conditions.[29] Two spectral regions were selected on the basis of the presence of characteristic bands of the glassy phases, coloring agents, and other compounds contained in the glass. Firstly, a wide interval of wave numbers was analyzed, 1800–600 cm^{-1} (623 data), the IR region in which the characteristic bands of glass appear, with the organic compounds appearing mainly between 1800 and 900 cm^{-1}, and also vitreous silica and alkali silicate glass were studied from 1200 to 850 cm^{-1} (337 data).[15,32] The principal components (PCs) were obtained using both the covariance data matrices (scaling by mean-centered data) and the correlation data matrices (scaling by unit variance). As occurred in previous research, results were better when PCA was performed on correlation data matrices, so the results shown and discussed here correspond to autoscaled data (centering data procedure). The applied autoscaling procedure gives the same relevance to each IR spectral region and spectral regions with small variation—no relevant IR bands—can acquire the same importance as large IR bands related to structural or compositional bands. Therefore, in this study, only IR bands containing the highest variability were chosen to apply PCA.[29–31] For 1800–600 cm^{-1}, no pattern distributions were detected when projecting the samples onto the space of the first PCs, and the score plots showed no relation between sample distribution and composition for all four color samples studied. The best results were obtained for the spectral region between 1250 and 600 cm^{-1}, shown in Table II. PCA was performed using the Statistical Product and Service Solutions program (SPSS, for Windows ver. 15, Chicago, IL).

Table II. PCA Results

Data matrix	Raman spectral region (cm^{-1})	PC	Variance account (%)	Variance accumulated (%)
Red	1250-600	PC1	83.2	83.2
		PC2	9.3	82.5
		PC3	4.6	97.1
Purple		PC1	90.8	90.8
		PC2	3.5	94.3
Blue		PC1	82.4	82.4
		PC2	14.7	97.1
		PC3	1.8	98.9
White		PC1	75.0	75.0
		PC2	16.7	91.7

III. Results and Discussion

The seven horse harness pendants were decorated with gilded copper by fire-gilding (also known as mercury-gilding) according to EDS results. This widespread method from the 12th to the 18th century is based on the application of an amalgam of gold and mercury, in which the mercury is burned off and the gold remains adhered to the metal object.[36] In fact, some traces of mercury were identified. Due to the extensive use of the fire-gilding the dating cannot be carried out using the gilding processes. Thus, the identification of workshops was carried out according to the composition of the enamels.

(1) Red Enamels

The general state of conservation of red enamels varies from one pendant to the next and even within the same pendant, with damage such as pits, cracks, and dark opaque areas often adjoining healthy, undamaged surfaces. Two chemometric analyses of red enamels (i.e., pendants 1, 4, 6, 7, and 11) were carried out on micro-ATR-FTIR data. However, an in-depth examination of the score plots of the first three PCs for the 1800–600 cm^{-1} interval showed a low total variance. In opposite to this, the highest quality information for discriminating samples was obtained using the interval between 1250 and 600 cm^{-1} (337 data). The score plots of the three PCs (Fig. 2) accounted for 97.1% of the total variance and PC1 (83.2%), PC2 (9.3%), and PC3 (4.6%) discriminated the sample into eleven groups (Table II).

In particular, the score plots of PC1 revealed that the distribution of clusters was not related to the analyses of each pendant, in fact, the highest score plots grouped some areas of the following pendants together: 1c, 4a–b, and 11b with high positive scores from pendants: 1a-b-d-e, 4c, 6, 7c, and 11a–c with more negative and zero scores. In addition, the PC2 score plots showed the total separation of the ATR-FTIR spectra collected on one area of pendant 11c (positive scores) from the rest of the samples (zero scores and slightly negative scores) [Fig. 2(a)]. Finally, PC3 score

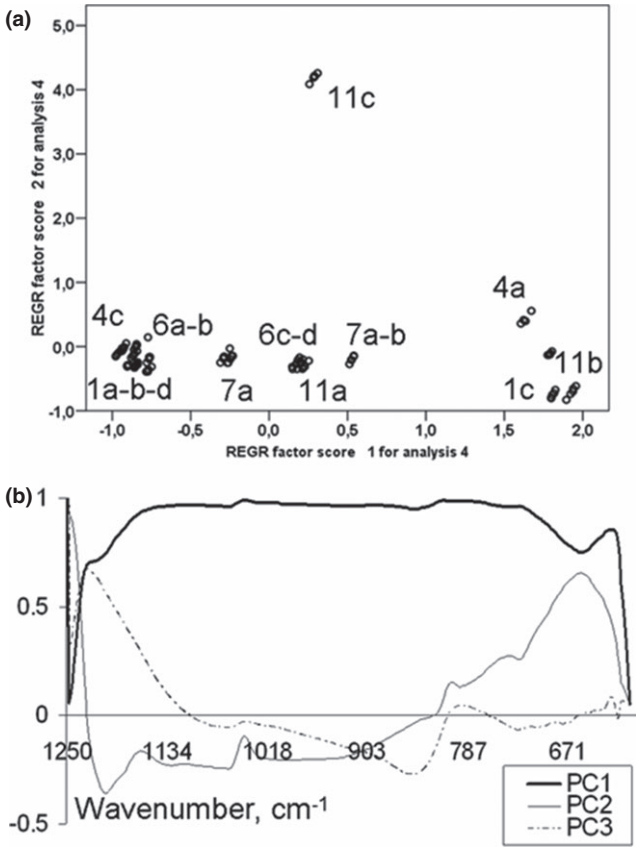

Fig. 2. PCA results for red enamels in the ATR-FTIR region between 1250 and 600 cm^{-1}: (a) Score plot of PC1 and PC2 and (b) loading plot of PC1, PC2, and PC3.

plots showed a slight separation of pendant 4 analyses with negative scores from the rest of the analyses, which were mainly located around zero, except for the ATR-FTIR spectral data for pendant 11c, which had the highest scores.

The analysis of the corresponding loadings for the first PC revealed that the spectral regions from 1151 to 721 cm^{-1} and the IR band at 668 cm^{-1} had high positive values, which were related to different glass networks and a changeable content of cobalt oxide[16] and for some areas of the pendants, i.e., 1c, 4a–b, 11b [Fig. 2(b)]. In addition, the PC2 gave high positive values to the IR band at 620 and 651 cm^{-1}, characteristic band of Cu–O and Mn–O (i.e., pyrolusite), respectively, and 804 cm^{-1}, which was attributed to the glass network on the basis of isolated tetrahedra, referred to as Q^0 by Colomban.[15,16] This cuprous oxide can be related to a changeable content due to the contamination from the metal base or from the copper-ruby glass composition of the pendants. The PC3 loading plots grouped samples according to the shift of the silicate IR band to a Q^1 structure (tetrahedra linked by a common oxygen atom, Si_2O_7), detecting IR bands at 943 cm^{-1} for pendants 4 and 7 [Fig. 2(b)].[7,15,17,32] Thus, the PC2 and PC3 loading plots indicated chemical modifications, i.e., an increase in the AsO_4^{3-} content at 830 cm^{-1} and Pb–O, and Q^0 and Q^1 species, which were related to processes of depolymerization of the glass network mentioned above.

Consequently, some altered surfaces of the red enamel from pendant 11 behaved differently in terms of microstructure and pyrolusite content. In particular, IR spectra for pendant 11 revealed Q^0 and Q^2 species (i.e., two bridging oxygens which form silicate chains located between ca. 1050 and 1100 cm^{-1}) and hence, this enamel showed some areas in a good state of conservation while others were altered as a result of depolymerization processes.[22] According to the literature, a high PbO content increases the degree of depolymerization of the silicate network[7]; it could increase the sensitivity to alteration processes in the enamels on pendants 1, 6 and some areas of pendant 11 owing to the higher Pb content (Table I). In fact, the chemical elements revealed a different composition; in particular, these pendants were alkali-lead (K–Pb) glass, while pendants 4 and 7 were mainly soda-lime and alkaline-earth (Na–Ca) glass. Consequently, glass weathering could occur and hence, ion exchanges could justify the low alkali and alkali-earth contents (Ca, K, Na, Mg) in some areas. These facts would suggest low production costs and consequently, poor quality glass, also corroborating the hypothesis about a manufacturing process in which the atmosphere is not controlled, due to the presence of copper-ruby.[5,11] Therefore, the control of the melting and cooling conditions is a key stage during the manufacturing process and must be taken into consideration.

To clarify the EDS analysis for these objects, ternary phase diagrams were compiled from elemental chemical quantification of Si–Na–Pb and K–Ca–Pb (Fig. 3). The first diagram showed clusters with similar proportions of Si and Na in the red enamels [Fig. 3(a)], but slightly different K, Ca, and Pb content; three clusters were distinguished in the second diagram [Fig. 3(b)]. In particular, pendant 7 was recognized because it had the lowest lead content, while pendants 1 and 4 were grouped together and separate from pendants 6 and 11, which had similar Ca content mainly. In addition, both diagrams showed the varied elemental composition of pendant 11 as indicated above. Tin oxide was also identified in pendant 7 as an opacifier (Table I).

(2) Purple Enamels

Similar chemometric analyses were carried out for the purple enamels for pendants 1, 10, and 11. In particular, visual examination using OM mainly showed problems of loss of material, cracks, and pits in some areas of pendants 1 and 10, which were analyzed in detail to identify the alteration mechanisms. The correlation extraction to the IR region between 1250 and 600 cm^{-1} (338 data) was more informative (Table II). Projection of the data samples from the original

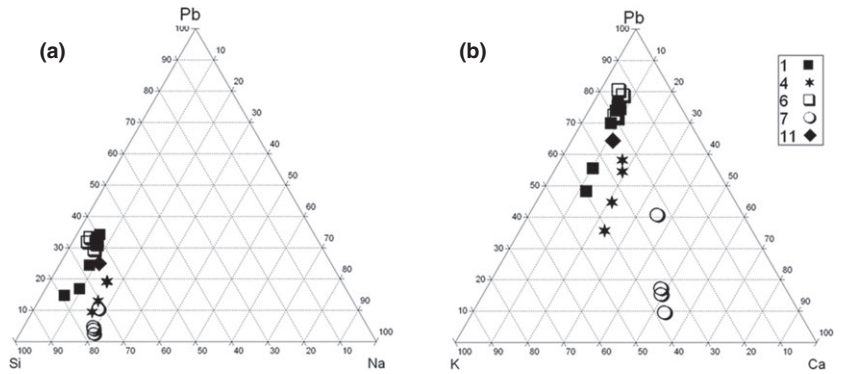

Fig. 3. Ternary phase diagrams of red enamels: (a) Si–Pb–Na and (b) K–Pb–Ca.

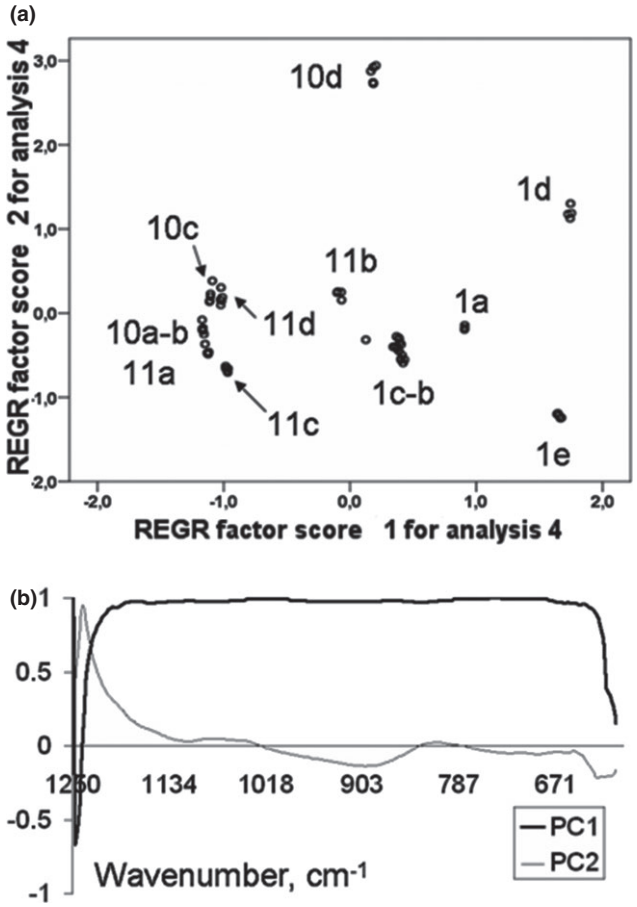

Fig. 4. PCA results for purple enamels in the ATR-FTIR region between 1250 and 600 cm^{-1}: (a) Score plot of PC1 and PC2 and (b) loading plot of PC1 and PC2.

space into the plane of the first two PCs revealed ten clear groups [Fig. 4(a)]. In particular, the score plots of both PCs grouped the spectra according to the objects analyzed, i.e., scattered analyses of pendant 1 (positive scores) were observed as opposed to negative score plots for pendants 10 and 11 for the PC1. Also, the PC2 mainly allowed us to discriminate pendant 10 (position d) from the rest of the analyses with a positive score. Thus, the PCA results showed higher degree of surface alteration for pendants 1 and 10. Due to the complexity of interpreting surface alterations and the clustering of samples according to the score plots, it was necessary to perform a detailed study of the loading plots and the greatest statistical loading for each PC.

The loading plot of the PC1 indicated a contribution of the whole spectral interval in grouping the samples from 1200 to 630 cm^{-1}, the region in which the main bands of the silicate networks appear [Fig. 4(b)]. We also performed an in-depth visual examination of this IR region, which revealed a slight shift of Si–O stretching modes at 925, 912, 946, and 930 cm^{-1} (associated to Q^1 species) for the different areas we studied of pendant 1. Consequently, a varied degree of surface alteration could be recognized for the pendants 1, 10, and 11. Furthermore, the loading plot of PC2 allowed the discrimination of spectra mainly due to the higher positive loading values of Mn–O band at 804 cm^{-1} (i.e., a purple ionic coloring agent[11]) and a slight shift of the asymmetric stretching mode Si–O–Si of silicate tetrahedra.[32] In particular, this shift was identified for the following areas: pendant 1d at 958 cm^{-1}; 10c–d at 943 cm^{-1}, both bands are attributed mainly to Q^1 species; pendant 11b at 871 cm^{-1} which is associated with a Q^0 structure; and 11d at 1035 cm^{-1}, where the activity of Q^2 species is expected. In addition, it is clear that the negative loading values of PC2 are related to the

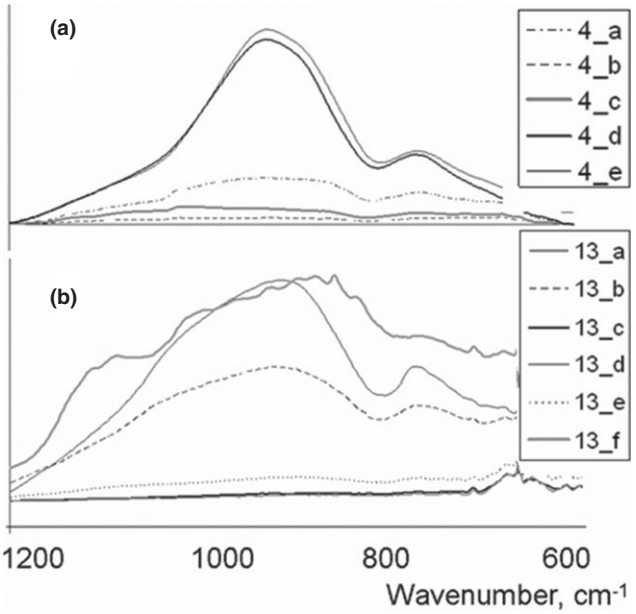

Fig. 5. ATR-FTIR spectra data for blue enamels of pendants (a) 4, and (b) 13.

content of Q^1 and copper oxides (as impurities) which were detected in some of the areas studied in pendant 1.

Therefore, PCA was unable to discriminate the ATR-FTIR spectra data according to the pendants analyzed, but a scattered distribution of the analyses was recognized. This suggested varying behavior of the different areas studied in the same enamel due to different composition and/or microstructure, which meant that a different degree of surface alteration could occur. According to Ricci, the proportion of Q^n species is susceptible to different firing temperatures and hence, the evolution of vibrational spectra of Q^1 could provide information about an irregular or nonconstant melting temperature during the manufacture of glass.[23] In fact, the different degree of alteration of areas of purple enamel and nonconstant melting temperature from pendants 1 and 10 were shown by the loading plot of PC1 and PC2, mainly associated with Q^0 and Q^1 species. However, the chemical composition studies did not show significant differences between the samples, except for a high chlorine content for pendant 10 and a slightly lower Pb–O content for pendant 11 (Table I). This suggests that the purple enamel had a microstructure and alteration mechanisms that were not influenced by the chemical composition, as we proposed for the red enamels, i.e., the high chlorine content could be responsible for the opaque aspects as a result of the presence of pits, fissures, cracks, and grooves in pendant 10. Moreover, the fact that the purple enamel from pendant 11 was in a good state of conservation was attributed to its polymerized structure as indicated above. Indeed, no conclusive results can be drawn from the detailed study of the distribution of analysis by ternary phase diagrams. The quantitative EDS analyses showed a similar content of the main oxides, except for a higher chloride content in pendant 10 (Table I).

(3) Blue Enamels

The visual examination of surface blue enamels from pendants 4, 6, 7, 11, and 13 showed decay manifested in the presence of dark and opaque enamels as well as loss of material. The detailed visual ATR-FTIR spectra revealed a different spectral signal for the different pendants and even for different areas of the same enamel; we observed a decrease and shift of IR bands around the silicate network region for the pendants (Fig. 5). We therefore decided to evaluate this region using PCA to clarify the decay mechanism at work.

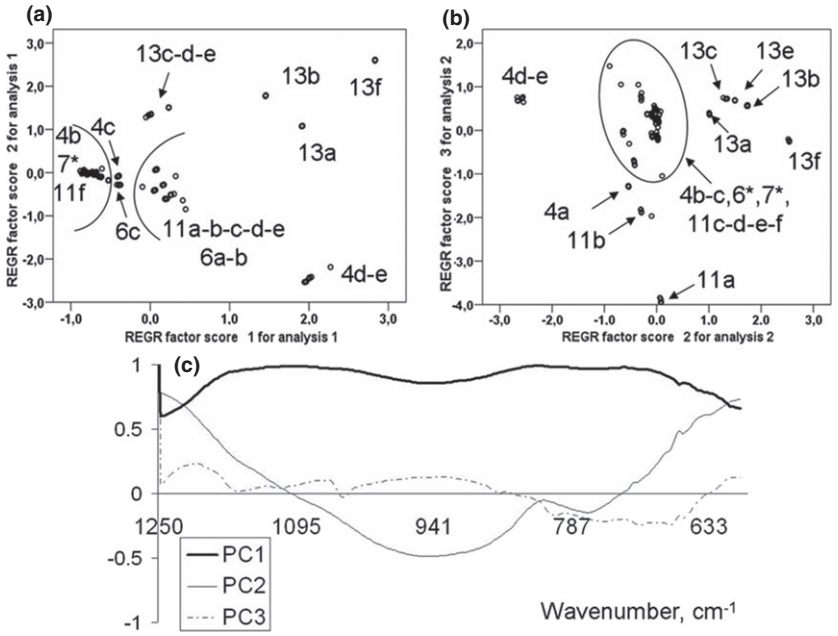

Fig. 6. PCA results for blue enamels in the ATR-FTIR region between 1250 and 600 cm^{-1}: Score plot (a) of PC1, PC2, (b) of PC2 and PC3 and (c) loading plot of PC1, PC2, and PC3.

As happened with the above chemometric analyses, the IR region between 1250 and 600 cm^{-1} (338 data) provided better discrimination between the samples. In fact, an in-depth assessment of the score plot of the three first PCs showed that the distribution of score plots of PC1 (82.4%) was mainly related to pendants 4 and 13 [Fig. 6(a)]. In particular, scattered clusters were identified for both pendants from negative to positive score plots and the rest of the analyses were located close to zero or slightly negative scores. Surprisingly, the score plot for PC2 and PC3, which accounted for only 16.5% of the total variance, improved the results [Fig. 6(b)]. The projection of the samples onto the spaces of the PC2 and PC3 showed the distribution of the samples in twelve groups mainly based on the different alteration of pendants 4 and 11 according to the OM study. In particular, some analyses of pendant 4 showed negative scores for PC2 and other areas of pendant 11 showed negative scores for PC3, while the rest of the samples were characterized with score values near zero for both PCs.

Again, the interpretation of the PCA results was difficult given that many spectral regions weighted the PCs as can be observed from the loading plots in Fig. 6(c). Despite this, the analysis of the loadings of the first PC revealed that IR regions such as 1125–1070 cm^{-1}, 840–800 cm^{-1}, and 740–700 cm^{-1} had large positive values due to the many changes in the silicate network for pendants 4 and 13. In addition, the loading plot of PC2 grouped the samples according to a contribution of the spectral interval of vibrations with zero, one, and two bridging oxygens (Q^0, Q^1, and Q^2) mainly for pendant 11. Finally, the negative loading plot of PC3 indicated the different proportion of cobalt (IR band at 668 cm^{-1}) and manganese oxide in the blue enamel of pendant 11 and the presence of Q^0 species. Consequently, the chemometric studies permitted the discrimination of samples according to glass weathering. In particular, different areas of blue enamel of pendant 4 showed a varied Q^n species; hence, some areas suffered alteration due to depolymerization processes, an effect confirmed by its high lead-oxide content. Similar results were found for the blue enamel from some altered areas of pendant 11, in which it showed total depolymerization (Q^0 species), producing ion exchanges of calcium and sodium, so corroborating the similar discussion for the red enamel for this pendant.

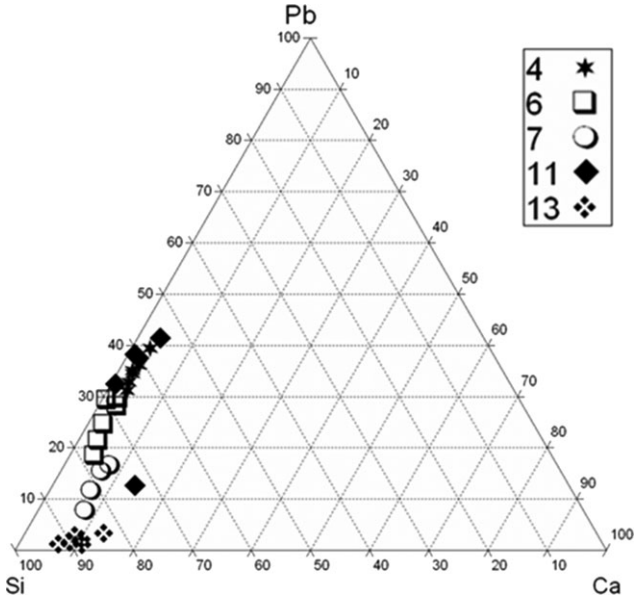

Fig. 7. Ternary phase diagram (Si–Pb–Ca) for blue enamels from pendants 4, 6, 7, 11, and 13.

The EDS results showed that the blue enamels were lead glass with a varied content of potassium, sodium, and calcium (Table I). In particular, the ternary phase diagram based on Si–Pb–Ca contents revealed the clustering of pendants mainly due to the lower proportion of Ca in pendant 13 and also the similar chemical composition of pendants 4 and 11 (Fig. 7) . As regards the coloring mechanism, the EDS analysis of blue enamels also showed cobalt as a pigment in pendants 4, 7, 11, and 13, although this chemical element was not detected in pendant 6. In addition, the EDS analysis showed a normal proportion of sodium and a strikingly low amount of lead in blue enamel 13, which could suggest different weathering behavior and a possible different origin from the rest of the objects.

As regards coloring agents, the presence of cobalt as a pigment (i.e., blue smalt) explained the blue color of the enamels from pendants 4, 7, 11, and 13. However, the absence of

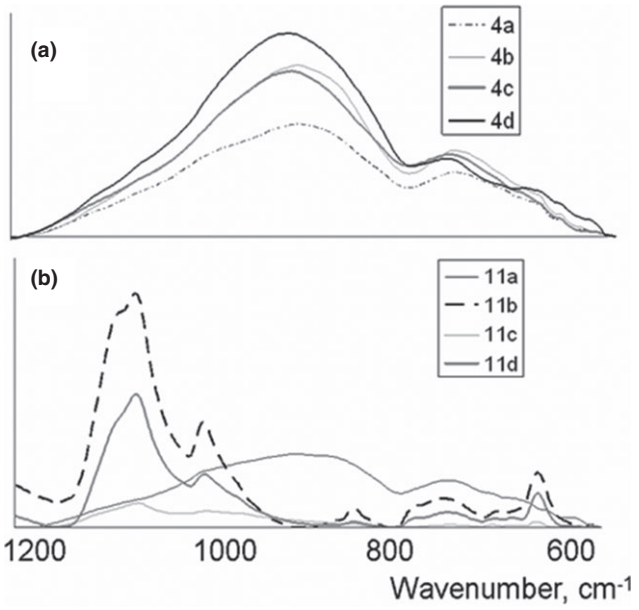

Fig. 8. Spectra data for white enamel from pendants: (a) 4; and (c) 11.

cobalt in the corresponding enamel from pendant 6 could suggest another ionic coloring mechanism, i.e., Fe(II) or Cu(II) ions to render blue glass, in fact, Fe(II) ion was the most frequent blue coloring agent in ancient glass-making.[11,21,38,39] In addition, the identification of traces of chrome only in this pendant corroborated the hypothesis that pendant 6 had a different historical origin from the other pendants (Table I).

(4) White Enamels

To compare the above PCA results on IR spectral data for red, purple, and blue enamels regarding the state of conservation and quality of manufacture, white enamels from pendants 4, 7, 11, and 13 were analyzed using similar methods to those mentioned above. The OM study showed many pits and dark impurities located inside the white enamels from pendants 4, 11, and 13, and cracks in pendant 7. In addition, the visual examination of IR spectra showed a significant difference between the analyses performed on each altered and each undamaged surface (Fig. 8). In particular, the study of each IR spectrum between 1250 and 600 cm^{-1} showed a shift of the Si–O stretching mode for pendants 11 and 13 for the areas studied, although this band showed a stable position and a decrease for pendants 4 and 7.

Due to the high complexity and wide range of spectra registered, PCA was performed. Two IR regions were analyzed, i.e., 1800–600 cm^{-1} and 1250–600 cm^{-1}, of which the second was more informative, as was expected (Table II). In particular, PCA results in 1250–600 cm^{-1} (338 data) allowed samples to be separated into fifteen groups [Fig. 9(a)]. In particular, the score plots for PC1 (75.0% of the total variance), showed that the white enamel from pendant 13 clearly differed from the rest of the samples with positive scores, while the corresponding enamel from pendant 11 was distinguished with a positive score for the PC2 (16.7% of the total variance).

The interpretation of loading plots clarified the above distribution of the pendants by projecting them onto the space of the first two PCs. The Fig. 9(b) showed that IR bands at 1176 cm^{-1}, 1070 cm^{-1}, and IR region 842–690 cm^{-1} had large positive values for PC1. The information for pendants 7 and 13 was therefore mainly related to the shift of Si–O stretching to Q^2 species and low Pb–O content, corroborating the good state of conservation for these areas as shown by the OM. In addition, the PC2 also showed the significant shift of silicate modes, and consequently the spectral region between 1160 and

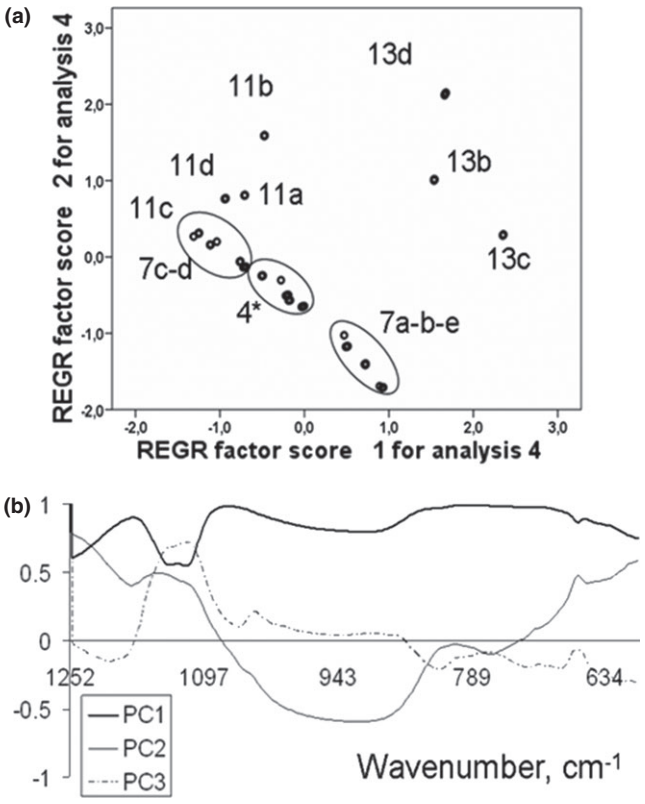

Fig 9. PCA results for white enamels in the ATR-FTIR region between 1250 and 600 cm^{-1}: (a) Score plot and (b) loading plot of PC1, PC2 and PC3.

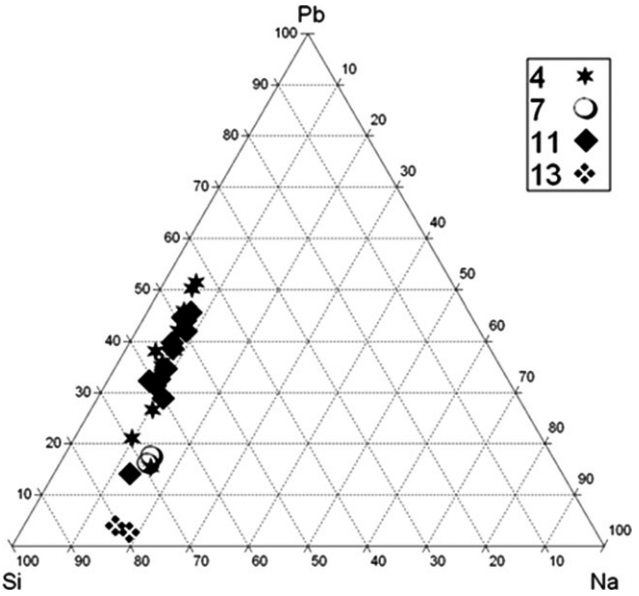

Fig. 10. Ternary phase diagram (Si–Pb–Na) for white enamels from pendants 4, 7, 11, and 13.

1110 cm^{-1} gave large positive values for the white enamel from pendant 11. Hence, the presence of Q^4 species was identified in this white enamel, so maintaining the high degree of polymerization in these areas. The projection into the plane of the first two PCs also showed the relative stability of the white enamels from pendants 4 and 7 compared with the variable silicon and lead content for pendants 11 and 13 (Table I). This could suggest that the white enamels had different composition or different durability properties.

In the main, the EDS results showed lead-glass for pendants 4, 7, and 11, but poor-lead enamel for pendant 13

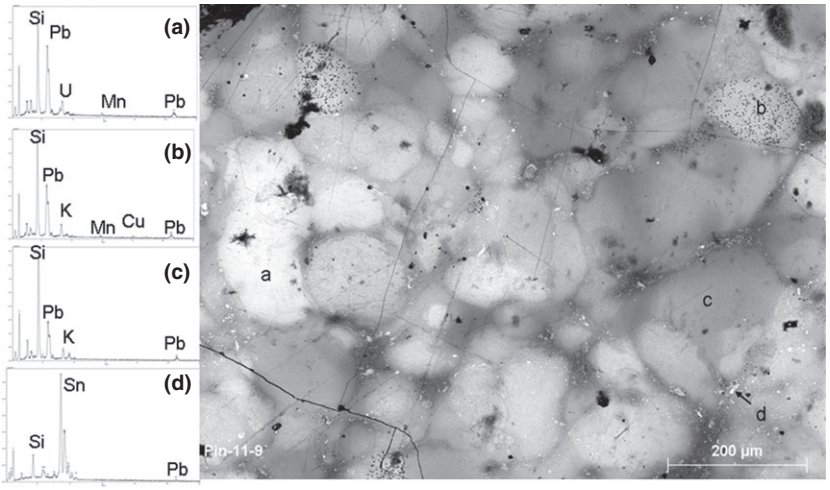

Fig. 11. BSE image and EDS analyses of the unaltered white enamel from pendant 11: (a) rich-uranium areas; (b) rich-lead areas; (c) poor-lead areas, and (d) small grains of tin oxides (5–15 µm).

(Table I). In addition, significantly higher content of tin opacifier was identified in pendant 7 and traces of uranium in pendant 4 and 11. In fact, the triangular diagram of Si–Pb–Na clearly revealed the similar composition of the white enamel from pendants 4 and 11, which were grouped close together and the separation of pendant 13 made of poor-lead glass (Fig. 10). Pendant 7 was located at an equidistant position between both groups due to its medium proportions of these chemical species.

In addition, the fact that uranium was only present in pendants 4 and 11 suggested that these two white enamels may have been manufactured using similar recipes. According to the literature, uranium has been used extensively in oxide form in glass-making since the 18th century owing to its brightness properties.[40,41] There is no structural evidence relating to the uranium content in these two white enamels, but the varied composition and a shift of the Si–O stretching mode in some areas of pendant 11 suggested depolymerization processes. The detailed study of SEM images (Fig. 11) showed areas of different composition in uranium, lead, and tin oxides, which caused the different ATR-FTIR spectra obtained due to its lower spatial resolution. The EDS results for the white enamel from pendant 13 also suggested a different origin due to the low proportion of lead and the fact that contaminants such as sulfates and chlorite were only present in this pendant, so confirming the archeological hypothesis of different sources based on stylistic criteria and comparison with the other pendants, which were attributed to Muslim culture from 13th century.[37] Moreover, the unusual composition as well as the presence of contaminants was evidence of alteration processes such as depolymerization, glass weathering, pits, cracks, etc.

IV. Conclusions

A novel nondestructive analytical methodology based on the combined use of PCA on micro-ATR-FTIR spectral data and chemical quantification using SEM-EDS allowed the discrimination of the different harness pendants according to the chemical composition, nanostructure and/or coloring mechanisms of enamels. In addition, the PCA results allowed the discrimination of a well-known harmful effect of glass weathering, i.e., depolymerization of glass networks, which was related to processes of ion exchanges. Moreover, this analytical methodology also allowed us to establish the different origins of these objects according to the composition of the enamels.

In particular, two workshops (named as group A and B) from an unknown historical period were identified as having manufactured pendants 6 and 13 separately on the basis of their composition. In fact, the decoration of pendant 6 was related to Christian designs of the extended traditional initial "E" of Isabel I, the Catholic Queen (1451-1504), in contrast to the Islamic decorations of the pendant 13.[37] Consequently, these two pieces could be contemporaries but from different workshops. Another workshop was responsible for the production of pendants 4 and 11, which probably dated between 1830 and 1940 as the presence of uranium attests (group C)[40,41] in spite of the reference that attributes these pieces to 15th century.[37] The composition of pendant 7 suggested that this object was prepared using recipes of red enamel similar to those used in group C. However, pendants 1 and 10 could not be attributed to any particular workshop or historical period, but their decoration could be attributed to the 14th or 15th century.[37] Nevertheless, the study of their microstructures and degrees of alteration suggested that both objects had suffered similar harmful effects as a result of inadequate use, storage, and/or exhibition since their manufacture, causing a similar state of conservation.

This analytical methodology therefore enabled us to perform an in-depth study of these pendants, which provided evidence and information about their possible age and origin. This evidence suggested that some of the pendants which had been thought to date from the 14th to 15th centuries were in fact of much more recent origin. It also allowed us to propose that two of the pendants (i.e., 4 and 11, which depicted coats of arms) may well have been produced in the same workshop, while the others were almost certainly the work of different craftsmen or the result of different enameling techniques.

Acknowledgments

This research was supported by Research Groups RNM-179 (Junta de Andalucía) and Spanish Science Ministry Project P08-RNM-04169. The authors gratefully acknowledge *Instituto de Patrimonio Cultural de España* (IPCE) and *Instituto Valencia de Don Juan* staffs for authorizing this research, and Dr. E. Manzano and A. Gómez for supporting this project. We thank M.A. García for helping us use the micro ATR-FTIR equipment at the Materials Laboratory of IPCE and Dr. L. Torres Zuñiga for the English revision.

References

[1]B. Messiga and M. P. Riccardi, "Alteration Behaviour of Glass Panes From the Medieval Pavia Charterhouse (Italy)," *J. Cult. Herit.*, **7** [4] 334–8 (2006).

[2]A. Climent-Font, A. Muñoz-Martin, M. D. Ynsa, and A. Zucchiatti, "Quantification of Sodium in Ancient Roman Glasses with Ion Beam Analysis," *Nucl. Instrum. Methods B*, **266** [4] 640–8 (2008).

[3]T. Pradell, J. Molera, N. Salvadó, and A. Labrador, "Synchrotron Radiation Micro-XRD in the Study of Glaze Technology," *Appl. Phys. A*, **99** [2] 407–17 (2010).

[4]B. Dal Bianco and U. Russo, "Basilica of San Marco (Venice, Italy/Byzantine Period): Nondestructive Investigation on the Glass Mosaic Tesserae," *J. Non-Cryst. Solids*, **358** [2] 368–78 (2012).
[5]N. Brun, L. Mazerolles, and M. Pernot, "Microstructure of Opaque Red Glass Containing Copper," *J. Mater. Sci. Lett.*, **10** [23] 1418–20 (1991).
[6]I. Borgia, B. Brunetti, I. Mariani, A. Sgamellotti, F. Cariati, P. Fermo, M. Mellini, C. Viti, and G. Padeletti, "Heterogeneous Distribution of Metal Nanocrystals in Glazes of Historical Pottery," *Appl. Surf. Sci.*, **185** [3–4] 206–16 (2002).
[7]S. Feller, G. Lodden, A. Riley, T. Edwards, J. Croskrey, A. Schue, D. Liss, D. Stentz, S. Blair, M. Kelley, G. Smith, S. Singleton, M. Affatigato, D. Holland, M. E. Smith, E. I. Kamitsos, C. P. E. Varsamis, and E. Ioannou, "A Multispectroscopic Structural Study of Lead Silicate Glasses Over an Extended Range of Compositions," *J. Non-Cryst. Solids*, **356** [6–8] 304–13 (2010).
[8]S. Akyuz, T. Akyuz, N. M. Mukhamedshina, A. A. Mirsagatova, S. Basaran, and B. Cakan, "Characterization of Ancient Glass Excavated in Enez (Ancient Ainos) Turkey by Combined Instrumental Neutron Activation Analysis and Fourier Transform. Infrared Spectrometry Techniques," *Spectrochim. Acta B*, **71–72**, 75–9 (2012).
[9]L. De Ferri, D. Bersani, A. Lorenzi, P. P. Lottici, V. Gezzalini, and G. Simon, "Structural and Vibrational Characterization of Medieval Like Glass Samples," *J. Non-Cryst. Solids*, **358** [4–6] 814–9 (2012).
[10]A. M. Pollard and C. Henron, *Archaeological Chemistry*. The Royal Society of Chemistry, Cambridge, 1996.
[11]J. M. Fernández-Navarro, *El Vidrio*, 1st edition. Consejo Superior de Investigaciones Científicas. Sociedad Española de Cerámica y Vidrio, Madrid, 1985.
[12]A. Duran, J. M. Fernandez Navarro, P. Casariego, and A. Juglar, "Optical Properties of Glass Coatings Containing Fe and Co," *J. Non-Cryst. Solids*, **82** [1–3] 391–9 (1986).
[13]M. Laczka and K. Cholewa, "Chromium, Cobalt, Nickel and Copper as Pigments of Sol-Gel Glasses," *J. Alloy. Compd.*, **218**, 77–85 (1995).
[14]A. Terczynska-Madej, K. Cholewa-Kowalska, and M. Laczka, "The Effect of Silicate Network Modifiers on Colour and Electron Spectra of Transition Metal Ion," *Opt. Mater.*, **32** [1] 1456–62 (2010).
[15]P. Colomban, "Raman Spectrometry, a Unique Tool to Analyze and Classify Ancient Ceramics and Glasses," *Appl. Phys. A*, **79** [16] 7–70 (2004).
[16]D. Jonynaite, J. Senvaitiene, A. Beganskiene, and A. Kareiva, "Spectroscopic Analysis of Blue Cobalt Smalt Pigment," *Vibr. Spectrosc.*, **52** [2] 158–62 (2010).
[17]S. Pérez-Villar, J. Rubio, and J. L. Oteo, "Study of Color and Structural Changes in Silver Painted Medieval Glasses," *J. Non-Cryst. Solids*, **354** [17] 1833–44 (2008).
[18]P. Ricciardi, P. Colomban, A. Tournié, M. Macchiarola, and A. Naceur, "A Non-Invasive Study of Roman Age Mosaic Glass Tesserae by Means of Raman Spectroscopy," *J. Archaeol. Sci.*, **36** [11] 2551–9 (2009).
[19]L. C. Prinsloo, A. Tournié, and P. Colomban, "A Raman Spectroscopic Study of Glass Trade Beads Excavated at Mapungubwe Hill and K2, two Archaeological Sites in Southern Africa, Raises Questions About the Last Occupation Date of the Hill," *J. Archaeol. Sci.*, **38** [12] 3264–77 (2011).
[20]P. Colomban, "The on-Site/Remote Raman Analysis with Mobile Instruments: A Review of Drawbacks and Success in Cultural Heritage Studies and Other Associated Fields," *J. Raman Spectrosc.*, **43** [11] 1529–35 (2012).
[21]B. Kırmızı, P. Colomban, and B. Quette, "On-Site Analysis of Chinese Cloisonné Enamels From Fifteenth to Nineteenth Centuries," *J. Raman Spectrosc.*, **41** [7] 780–90 (2010).
[22]P. Colomban and A. Tourni, "On-Site Raman Identification and Dating of Ancient/Modern Stained Glasses at the Sainte-Chapelle, Paris," *J. Cult. Heritage*, **8** [3] 242–56 (2007).
[23]C. Ricci, C. Miliani, F. Rosi, B. G. Brunetti, and A. Sgamellotti, "Structural Characterization of the Glassy Phase in Majolica Glazes by Raman Spectroscopy: A Comparison Between Renaissance Samples and Replica Processed at Different Temperatures," *J. Non-Cryst. Solids*, **353** [11–12] 1054–9 (2007).
[24]L. Raffaelly, B. Champagnon, N. Ollier, and D. Foy, "IR and Raman Spectroscopies, a Way to Understand How the Roman Window Glasses Were Made?" *J. Non-Cryst. Solids*, **354** [2–9] 780–6 (2008).
[25]T. A. Sidorov, "Vibration Spectra of Three-Component Silicate Glasses and the Role of Chemical Elements in the Structure of Glass," *J. Appl. Spectr.*, **7** [3] 258–61 (1967).
[26]G. Musumarra and M. Fichera, "Chemometrics and Cultural Heritage Chemometrics and Intelligent Laboratory Systems," *Chemometr. Intell. Lab*, **44** [1] 363–72 (1998).
[27]P. Fermo, E. Delnevo, M. Lasagni, S. Polla, and M. de Vos, "Application of Chemical and Chemometric Analytical Techniques to the Study of Ancient Ceramics From Dougga (Tunisia)," *Microchem. J.*, **88** [2] 150–9 (2008).
[28]M. A. Rogerio-Candelera, V. Jurado, L. Laiz, and C. Saiz-Jimenez, "Laboratory and in Situ Assays of Digital Image Analysis Based Protocols for Biodeteriorated Rock and Mural Paintings Recording," *J. Archaeol. Sci.*, **38** [10] 2571–8 (2011).
[29]E. Manzano, J. Romero-Pastor, N. Navas, L. R. Rodríguez-Simón, and C. Cardell, "A Study of the Interaction Between Rabbit Glue Binder and Blue Copper Pigment Under UV Radiation: A Spectroscopic and PCA Approach," *Vib. Spectroscop.*, **53** [2] 260–8 (2010).
[30]N. Navas, J. Romero-Pastor, E. Manzano, and C. Cardell, "Raman Spectroscopic Discrimination of Pigments and Tempera Paintmodel Samples by Principal Component Analysis on First-Derivative Spectra," *J. Raman Spectrosc.*, **41** [11] 1196–203 (2010).
[31]J. Romero-Pastor, N. Navas, S. Kuckova, A. Rodríguez-Navarro, and C. Cardell, "Collagen-Based Proteinaceous Binder-Pigment Interaction Study Under UV Ageing Conditions by MALDI-TOF-MS and Principal Component Analysis," *J. Mass Spectrom.*, **47** [3] 322–30 (2012).
[32]S. A. MacDonald, C. R. Schardt, D. J. Masiello, and J. H. Simmons, "Dispersion Analysis of FTIR Reflection Measurements in Silicate Glasses," *J. Non-Cryst. Solids*, **275** [1–2] 72–82 (2000).
[33]P. Colomban, "Polymerisation Degree and Raman Identification of Ancient Glasses Used for Jewellery, Ceramics Enamels and Mosaics," *J. Non-Cryst. Solids*, **323** [1–3] 180–7 (2003).
[34]J. Sterpenich and G. Libourel, "Water Diffusion in Silicate Glasses Under Natural Weathering Conditions: Evidence From Buried Medieval Stained Glasses," *J. Non-Cryst. Solids*, **352** [50–51] 5446–51 (2006).
[35]M. Gulmini, M. Pace, G. Ivaldi, M. N. Ponzi, and P. Mirti, "Morphological and Chemical Characterization of Weathering Products on Buried Sasanian Glass From Central Iraq," *J. Non-Cryst. Solids*, **355** [31–32] 1613–21 (2009).
[36]V. Corregidor, L. C. Alves, N. P. Barradas, M. A. Reis, M. T. Marques, and J. A. Ribeiro, "Characterization of Mercury Gilding Art Objects by External Proton Beam," *Nucl. Instrum. Meth. B*, **269** [24] 3049–53 (2011).
[37]M. L. Martín Ansón, "La Colección de Pinjantes y Placas de Arnés Medievales del Instituto Valencia de Don Juan en Madrid," *Colección de Estudios, Universidad Autónoma de Madrid*, **96**, 538–45, (2004).
[38]P. Mirti, P. Davit, and M. Gulmini, "Colourants and Opacifiers in Seventh and Eighth Century Glass Investigated by Spectroscopic Techniques," *Anal. Bioanal. Chem.*, **372**, 221–9 (2002).
[39]R. Arletti, S. Quartieri, G. Vezzalini, G. Sabatino, M. Triscari, and M. A. Mastelloni, "Archaeometrical Analyses of Glass Cakes and Vitreous Mosaic Tesserae From Messina (Sicily, Italy)," *J. Non-Cryst. Solids*, **354** [45–46] 4962–9 (2008).
[40]R. Procházka, V. Ettler, V. Goliáš, M. Klementová, M. Mihaljevica, O. Šebek, and L. Strnad, "A Comparison of Natural and Experimental Long-Term Corrosion of Uranium-Colored Glass," *J. Non-Cryst. Solids*, **355** [43–44] 2134–42 (2009).
[41]D. Strahan, "Uranium in Glass, Glazes and Enamels: History, Identification and Handling," *Stud. Conserv.*, **46** [3] 181–95 (2001). □